INTERNATIONAL JOURNAL FOR NUMERICAL METHODS IN FLUIDS
Int. J. Numer. Meth. Fluids 2007; **54**:1131–1149
Published online 23 January 2007 in Wiley InterScience (www.interscience.wiley.com). DOI: 10.1002/fld.1424

Efficient retrieval of the thermo-acoustic flame transfer function from a linearized CFD simulation of a turbulent flame

J. F. van Kampen*,†, J. B. W. Kok and Th. H. van der Meer

Department of Thermal Engineering, University of Twente, P.O. Box 217, 7500 AE Enschede, The Netherlands

SUMMARY

The stability of thermo-acoustic pressure oscillations in a lean premixed methane-fired generic gas turbine combustor is investigated. A key element in predicting the acoustically unstable operating conditions of the combustor is the flame transfer function. This function represents the dynamic relationship between a fluctuation in the combustor inlet conditions and the flame's acoustic response. A transient numerical experiment involving spectral analysis in computational fluid dynamics (CFD) is usually conducted to predict the flame transfer function. An important drawback of this spectral method application to numerical simulations is the required computational effort. A much faster and more accurate method to calculate the transfer function is derived in this paper by using a most important basic assumption: the fluctuations must be small enough for the system to behave linear. This alternative method, which is called the *linear coefficient method*, uses a linear representation of the unsteady equations describing the CFD problem. This linearization is applied around a steady-state solution of the problem, where it can consequently describe the dynamics of the system. Finally, the flame transfer function can be calculated from this linear representation. The advantage of this approach is that one only needs a steady-state solution and linearization of the unsteady equations for calculating a dynamic transfer function, i.e. no time-consuming transient simulations are necessary anymore. Nevertheless, as a consequence of the large number of degrees of freedom in a CFD problem, an extra order reduction step needs to be performed prior to calculating the transfer function from the linear representation. Still, the linear coefficient method shows a significant gain in both speed and accuracy when calculating the transfer function from the linear representation as compared to a spectral analysis-based calculation. Hence, this method gives a major improvement to the application of the flame transfer function as a thermo-acoustic design tool. Copyright © 2007 John Wiley & Sons, Ltd.

Received 18 August 2006; Revised 5 November 2006; Accepted 12 November 2006

KEY WORDS: thermo-acoustics; state space; reduction methods

*Correspondence to: J. F. van Kampen, Siemens AG, PG, P.O. Box 10 17 5545466 Muelheim a.d. Ruhr, Germany.
†E-mail: jaapvankampen@gmail.com

Contract/grant sponsor: EU

1. INTRODUCTION

The dynamic relationship between a small fluctuation in the inlet conditions of a combustor and the resulting heat release rate perturbation of the flame is called the flame transfer function. This transfer function can be obtained from measurements [1–3], analytical models [4] and from transient computational fluid dynamics (CFD) simulations [5]. In CFD simulations, the inlet quantities of the combustor are perturbed by an excitation signal (white noise, sine, step function, etc.). Simultaneously, the response of the flame in terms of the volume-integrated heat release rate Q is monitored. The acoustic compactness of a flame allows this 'lumped' approach, in which the acoustic monopole sound source produced by the flame is volume integrated into a single point source.

With the transient data of the excitation and the response of the flame, a flame transfer function in the frequency domain can be constructed using Fourier transformation. Many spectral problems are involved in this procedure such as leakage, aliazing, lack of accuracy and frequency resolution, etc. Moreover, one always makes a truncation error in the time discretization scheme. Another big disadvantage of this method is the computational effort required to obtain an accurate flame transfer function with a reasonable frequency resolution.

In the numerical experiment, the amplitude of the excitation is usually small to have a linear response of the system (this is one of the basic requirements of the use of a transfer function and of spectral analysis). However, this linear response can be obtained *directly* by linearization of the unsteady equations that describe the CFD problem around a steady-state solution. Subsequently, the flame transfer function can be calculated from this linear representation. This linear representation is cast into a more general form: the *state-space system*. State-space systems are typically used in control engineering to describe dynamical systems.

Typically, the order of a linear representation of a CFD problem is larger than $\mathcal{O}(10^6)$. This large order requires an order reduction step to be applied prior to using the representation for calculating the transfer function. The combination of the state-space method and the order reduction method is called the *linear coefficient method*. With this method, the transfer function can be calculated faster and more accurately than with the conventional transient methods.

By its definition, the linear coefficient method yields linear transfer functions. This also applies to transfer functions constructed from an experimentally or numerically obtained time series and transferred to the frequency domain by spectral analysis. Due to this limitation the linear coefficient method is valid for small fluctuations and useful for linear controller design for combustion instabilities. Nonlinear saturation effects occurring in the limit cycle of combustion instabilities cannot be predicted by the method in its current form. An overview of linear ranges and nonlinear saturation effects for turbulent premixed combustion can be found in [6].

The intention of the current paper is to compare the linear coefficient method with a conventional CFD method, not to validate the conventional CFD method with experiments. Hence, in this paper a comparison is made between results based on the linear coefficient method combined with steady RaNS, and the unsteady RaNS (URaNS) approach. Flame transfer function modelling on basis of the URaNS approach has been compared to experimental results in literature by several authors (see, for example, [5, 7]). The application of the URaNS approach is justified when the turbulent fluctuations occur at a much smaller time scale than the periodic fluctuations, i.e. the characteristic frequency at which the turbulent fluctuations occur ($\sim \varepsilon/k$ when the k–ε turbulence model is used) is much higher than the frequency of the periodic fluctuation. When this requirement is met, the turbulence structure is unaffected by the unsteadiness. For the calculation of a flame transfer

DOI: 10.1002/fld

function of a turbulent flame, meeting this requirement is usually not a problem. As a result of the large Reynolds numbers, the time scale of the turbulent fluctuations is very small. In addition to that, the time scale of the periodic features is relatively large, since the maximum frequency of interest for the flame transfer function is in general relatively low (<500 Hz).

Since RaNS codes are designed to solve the total quantities, small perturbations are subjected to a relatively high numerical damping. With the adaptation of the equations which it acts upon, the linear coefficient method can also be applied to a laminar CFD code to calculate the dynamic behaviour of laminar flames. With some more effort, one could also apply it to large Eddy simulation (LES), in which the coupling between the periodic features and the turbulence is present and the numerical dissipation is much less than in RaNS simulations. The basic requirement of the method is that a steady state can be defined. In LES, this steady state could be an averaged solution. Using the coefficients at this averaged solution, a state-space representation can be constructed again. All spatial couplings are also included in the linear coefficient method. Therefore, it is also able to predict spatial flow structures, such as vortices.

In the next section, the state-space representation of the unsteady CFD equations is discussed. Moreover, as an example of the ability of the state-space representation to describe dynamical systems, the approach is applied to a simple mass–spring–damper system. Subsequently, the implicitly restarted Lanczos method is discussed. This method is used as an order reduction method. Finally, the combination of both methods will be applied to a simple RaNS CFD simulation involving combustion. This yields the flame transfer function of the numerical flame in this simulation. The speed and accuracy of the linear coefficient method are compared to the conventional spectral analysis method. This will clearly show the benefits of the linear coefficient method.

2. STATE-SPACE REPRESENTATION

The unsteady equations that are solved in a CFD simulation can be written as

$$\frac{\partial \psi_i}{\partial t} = f(\psi_1, \psi_2, \ldots, \psi_n), \quad i = 1, 2, \ldots, n \tag{1}$$

in which ψ_i are the variables in the problem, n equals the number of variables and t indicates time. The index i is a unique number, indicating an *independent* variable at a node. Since each independent variable is present at each node, the variable number i is defined as

$$i = n_{\text{var}}(i_{\text{node}} - 1) + i_{\text{var}} \tag{2}$$

in which i_{var} indicates the independent variable number (ranging from 1 to n_{var}, the number of independent variables at a node), and i_{node} is the node number (ranging from 1 to n_{node}, the number of nodes).

Solving Equation (1) for $f = 0$ yields the steady-state values of the independent variables. Subsequently, small perturbations ψ_i' around these steady-state values $\bar{\psi}_i$ are considered (e.g. $\psi_i = \bar{\psi}_i + \psi_i'$). Linearization of the resulting equations yields the following equations:

$$\frac{\mathrm{d}\psi_i'}{\mathrm{d}t} = \sum_{j=1}^{n} a_{ij}\psi_j', \quad i = 1, 2, \ldots, n \tag{3}$$

DOI: 10.1002/fld

in which a_{ij} are the coefficients representing the linear relationship between a fluctuation in ψ_j and the rate of increase in time of ψ_i. Inserting the coefficients in a system matrix **A**, Equation (3) can be written as

$$\frac{\mathrm{d}\mathbf{\Psi}'}{\mathrm{d}t} = \mathbf{A}\mathbf{\Psi}' \tag{4}$$

The coefficient matrix **A** contains the linear coefficients a_{ij} evaluated at the steady state $\bar{\psi}_i$. The vector $\mathbf{\Psi}'$ is the vector with the independent variables $\{\psi'_1, \psi'_2, \ldots, \psi'_n\}^{\mathrm{T}}$. The coefficient matrix includes the coupling between the nodes. This coupling comes from the discretized spatial derivatives in the equations (multiple nodes contribute to the gradient at a specific point).

For CFD problems the matrix **A** will be very sparse. For a single-step combustion simulation with a finite rate combustion model, typically 11 equations per node are solved ($n_{\mathrm{var}} = 11$). These equations are solved at n_{node} nodes. Assuming that each node is coupled to maximum $c = 20$ other nodes, the sparsity (non-zero elements divided by total number of elements) of the matrix **A** (with dimensions $n_{\mathrm{var}}n_{\mathrm{node}} \times n_{\mathrm{var}}n_{\mathrm{node}}$) equals

$$S = \frac{(c+1)n_{\mathrm{var}}(n_{\mathrm{var}}n_{\mathrm{node}})}{n_{\mathrm{var}}^2 n_{\mathrm{node}}^2} = \frac{(c+1)}{n_{\mathrm{node}}} \tag{5}$$

For $c = 20$ and $n_{\mathrm{node}} = 25\,000$, the sparsity is only 0.084%. Note that the sparsity decreases for increasing number of nodes, since obviously the average bandwidth of the matrix, determined by c, is approximately constant in case of a regular mesh. Consequently, relatively less non-zero coefficients are encountered for larger problems.

When inlet quantities of the system are perturbed, these quantities should be included in the unsteady equations. It is assumed that only one input variable is fluctuated. The unsteady part due to a fluctuating inlet variable ϕ' is linearized and added to Equation (4):

$$\frac{\mathrm{d}\mathbf{\Psi}'}{\mathrm{d}t} = \mathbf{A}\mathbf{\Psi}' + \mathbf{B}\phi' \tag{6}$$

in which **B** is a vector describing the linear influence of ϕ'.

For flame transfer function calculations, the single output of the system will be the volume-integrated unsteady heat release rate. This unsteady heat release rate Q' is a function of the unsteady variables $\mathbf{\Psi}'$ and of the fluctuating inlet variable ϕ'. This function can be linearized, resulting in the following expression:

$$Q' = \mathbf{C}\mathbf{\Psi}' + D\phi' \tag{7}$$

in which **C** is a vector and D is a scalar, both containing coefficients describing the linear influence on the equation for the unsteady heat release rate.

The matrix **A**, vectors **B** and **C** and the scalar D in Equations (6) and (7) describe the linear system in a state-space formulation. The sizes of these matrices are shown schematically in Figure 1. In this figure, the matrices for a single input, single output (SISO) system are shown, such that $m = 1$ and $p = 1$, respectively. The state-space systems considered in this paper are of this type. Moreover, the size of the system is denoted as n.

Assuming a harmonic time-dependence $\exp(\mathrm{i}\omega t)$ of the fluctuating quantities of Equations (6) and (7), the transfer function H between the input ϕ' and the output Q' at a specific angular

DOI: 10.1002/fld

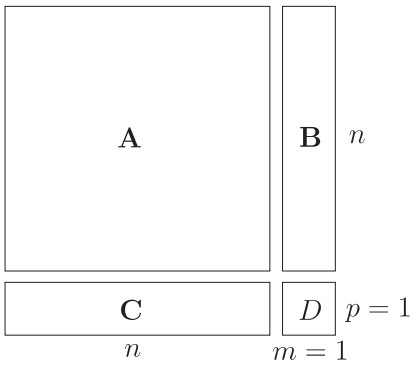

Figure 1. Schematic overview of the state-space matrices for a SISO system.

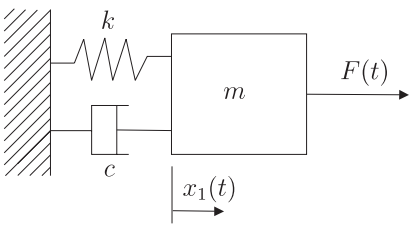

Figure 2. Mass–spring–damper system used in the example of the state-space approach.

frequency ω can be calculated as

$$H(\omega) = \frac{Q'}{\phi'} = \mathbf{C}(\mathrm{i}\omega\mathbf{I} - \mathbf{A})^{-1}\mathbf{B} + D \tag{8}$$

in which $\mathbf{I}$ is the identity matrix and i is the imaginary unit. So when the state-space matrices $\mathbf{A}$, $\mathbf{B}$, $\mathbf{C}$ and D are obtained by linearization around a certain steady-state solution of the unsteady equations of the system, the transfer function at any frequency ω can be determined with Equation (8). Using this method, there are *no* truncation errors in time, in contrast to the transfer function obtained from a transient calculation.

Example

To show the ability of the state-space representation to describe dynamical systems, it will be applied to the simple mass–spring–damper system shown in Figure 2.

The equations describing the dynamics of this system can be written as

$$\frac{\partial x_1}{\partial t} = x_2 \tag{9}$$

$$\frac{\partial x_2}{\partial t} = -\frac{k}{m}x_1 - \frac{c}{m}x_2 + \frac{1}{m}F \tag{10}$$

DOI: 10.1002/fld

where m, k and c are the mass, the spring constant and the friction constant, respectively. For this simple system, the steady-state solution does not influence the dynamic behaviour of the system. Therefore, the linearized system is similar to the system of Equations (9) and (10), with the variables x_1, x_2 and F replaced by their perturbed versions: x_1', x_2' and F'.

With Equations (9) and (10) the state-space system with output $y' = x_1'$ can be constructed as

$$\begin{bmatrix} \dfrac{\partial x_1'}{\partial t} \\ \dfrac{\partial x_2'}{\partial t} \end{bmatrix} = \begin{bmatrix} 0 & 1 \\ -\dfrac{k}{m} & -\dfrac{c}{m} \end{bmatrix} \begin{bmatrix} x_1' \\ x_2' \end{bmatrix} + \begin{bmatrix} 0 \\ 1/m \end{bmatrix} F' \tag{11}$$

$$y' = [1 \;\; 0][x_1' \;\; x_2']^{\mathrm{T}} + 0 \cdot F' \tag{12}$$

Having constructed the state-space system, the matrices **A**, **B**, **C** and D are known and can be inserted in Equation (8) to calculate the transfer function $H_e = y'/F'$ at a specific frequency ω. Figure 3 shows the expected amplitude and phase of this transfer function. The frequency is normalized by the eigenfrequency of the undamped system, $f_0 = (1/2\pi)\sqrt{k/m}$. The transfer function is plotted at three different values for the relative damping coefficient $\zeta = c/4\pi m f_0$.

It can be seen that representing the dynamical system with a state-space formulation provides a structured approach to calculate a specific transfer function. The same approach will now be applied to a much higher-order system, i.e. a CFD problem.

When applied to CFD problems, the order of the linear model is equal to the product of the number of nodes in the mesh and the number of independent variables that are solved at each node ($= n_{\mathrm{var}} n_{\mathrm{node}}$). For medium-sized systems (up to $\mathcal{O}(10^3)$), the transfer function can be explicitly calculated from the state-space matrices using Equation (8).

One of the operations included in Equation (8) is an inverse operator, acting on the coefficient matrix **A**. When the order of **A** is large, this inverse cannot be evaluated directly anymore due to

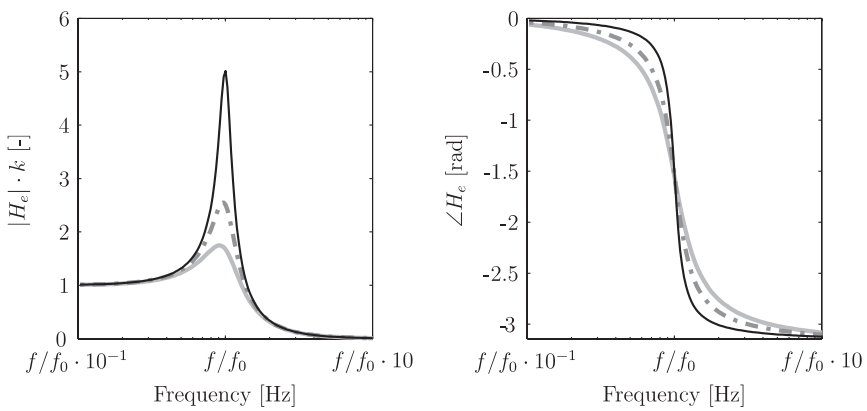

Figure 3. Transfer functions of mass–spring–damper system for different values of the relative damping coefficient. —, $\zeta = 0.1$; _ _, $\zeta = 0.2$; ——, $\zeta = 0.3$.

DOI: 10.1002/fld

memory and CPU time limitations. To calculate a transfer function for large systems, the state-space system itself is reduced in order by a reduction technique, which approximates the original system by a reduced order system. The technique removes insignificant information from the matrices. In the next section, it is shown how the state-space model can be reduced using the implicitly restarted and shifted Lanczos method.

3. REDUCTION METHODS

With reduction techniques the full state-space system (Equations (6) and (7)) is approximated by a dimensionally smaller state-space system of the form

$$\frac{\mathrm{d}\hat{\boldsymbol{\Psi}}'}{\mathrm{d}t} = \hat{\mathbf{A}}\hat{\boldsymbol{\Psi}}' + \hat{\mathbf{B}}\phi' \tag{13}$$

$$Q' = \hat{\mathbf{C}}\hat{\boldsymbol{\Psi}}' + D\phi' \tag{14}$$

in which the matrices with the hats are low-dimensional projections of their full counterparts. For an overview of reduction methods for large-scale dynamic systems, see [8, 9].

To obtain the reduced order system from the original system, $\boldsymbol{\Psi}'$ is approximated by $\mathbf{Q_k}\hat{\boldsymbol{\Psi}}'$, where $\mathbf{Q_k}$ is an orthonormal[‡] projector matrix of size $n \times k$, in which k is the order of the reduced model. Substituting this expression for $\boldsymbol{\Psi}'$ into the original state-space system, premultiplying the first equation with $\mathbf{Q_k^T}$, the following system is obtained:

$$\frac{\mathrm{d}\hat{\boldsymbol{\Psi}}'}{\mathrm{d}t} = \mathbf{Q_k^T}\mathbf{A}\mathbf{Q_k}\hat{\boldsymbol{\Psi}}' + \mathbf{Q_k^T}\mathbf{B}\phi' \tag{15}$$

$$Q' = \mathbf{C}\mathbf{Q_k}\hat{\boldsymbol{\Psi}}' + D\phi' \tag{16}$$

Hence, $\hat{\mathbf{A}} = \mathbf{Q_k^T}\mathbf{A}\mathbf{Q_k}$, $\hat{\mathbf{B}} = \mathbf{Q_k^T}\mathbf{B}$ and $\hat{\mathbf{C}} = \mathbf{C}\mathbf{Q_k}$.

The problem is now reduced to finding the orthonormal projector $\mathbf{Q_k}$. This is done with the Lanczos method [10], which, in its origin, is an inexpensive, iterative method to obtain a few largest and/or smallest eigenvalues of a matrix.

The general unsymmetrical version of the Lanczos method is explained in Appendix A (see also Golub and van Loan [11]). In the next section, it is shown how the method can serve as a state-space model reduction tool. After this, two methods are presented which can be used to overcome the following consequences of a poor starting vector:

(1) Due to a poorly chosen starting vector of the Lanczos iteration a stable full system can be transformed into an unstable reduced system. One can implicitly modify the matrix $\mathbf{Q_k}$ and pass immediately to a stable version of the reduced model. This procedure is called the implicitly restarted Lanczos method (see Grimme *et al.* [10]).
(2) By 'shifting' the coefficient matrix a so-called breakdown of the procedure can be prevented. Moreover, a better approximation around a chosen frequency is obtained.

[‡]A matrix $\mathbf{A}$ is orthonormal iff $\mathbf{A}^\mathrm{T}\mathbf{A} = \mathbf{I}$. This implies that $\mathbf{A}^\mathrm{T} = \mathbf{A}^{-1}$.

DOI: 10.1002/fld

3.1. Lanczos and model reduction

The idea is to use the Lanczos method to match the *moments* of the transfer function of the linear unreduced system with the reduced system. With the Lanczos method the matching of the moments will be done *without* explicitly calculating these moments. The advantage of this will become clear later in this section.

The moments of the transfer function are the coefficients of a power series expansion of $H(s)$. To obtain an expansion around $\sigma = \infty$, the initial value theorem known from the Laplace transformation is used

$$\lim_{s\to\infty} sG(s) = \lim_{t\to 0} g(t) \tag{17}$$

where $G(s)$ is the Laplace transform of $g(t)$. The expansion around $\sigma = \infty$ can thus be obtained by letting the time t go to zero in the inverse Laplace transform of $G(s) = H(s)/s$. This inverse Laplace transform can be calculated as

$$g(t) = \mathscr{L}^{-1}\left\{\frac{H(s)}{s}\right\} = \int_{t=0}^{t} \mathbf{C}\mathrm{e}^{\mathbf{A}t}\mathbf{B}\,\mathrm{d}t \tag{18}$$

Expanding this expression around $t = 0$ yields

$$g(t) = \sum_{j=1}^{\infty} \mathbf{C}\mathbf{A}^{j-1}\mathbf{B}\frac{t^j}{j!} \tag{19}$$

Using now the Laplace identity $\mathscr{L}\{t^n\} = n!/s^{n+1}$ the power series expansion for $H(s)$ around $\sigma = \infty$ can be obtained by Laplace transforming expression 19, yielding

$$H(s) = sG(s) = \sum_{j=1}^{\infty} \mathbf{C}\mathbf{A}^{j-1}\mathbf{B}s^{-j} \tag{20}$$

which results in the following expression for the moments (known as Markov parameters):

$$\eta_j(\sigma = \infty) \equiv \mathbf{C}\mathbf{A}^{j-1}\mathbf{B} \tag{21}$$

By matching as many moments as possible, the reduced system gives an approximation of the full system.

With the general Lanczos method the expansion around $\sigma = \infty$ will be matched. This means that the moments of Equation (21) are matched. In principle, one can also simply calculate the moments and obtain a lower-order expression for the transfer function. This would not be very computationally or memory expensive, since it only requires repeated matrix vector multiplications. However, the computation of these moments has shown to be numerically problematic [12], since the powers of the eigenvalues of $\mathbf{A}$ grow exponentially fast. This is the reason why the Lanczos method is used: it matches the moments of the transfer function expansion, without explicitly calculating the moments, but by projecting the state-space matrices on a reduced space.

The reduced state-space system that is obtained by projecting the original system with the orthonormal projector matrices $\mathbf{P_k}$ ($= \mathbf{Q_k}^{-\mathrm{T}}$, see Appendix A) and $\mathbf{Q_k}$ has the same first $2k$ moments

DOI: 10.1002/fld

as the original state-space system. This can be shown by noting that for any polynomial function $\mathscr{P}$ there holds

$$\mathscr{P}(\mathbf{A})\mathbf{Q_k} = \mathbf{Q_k}\mathscr{P}(\hat{\mathbf{A}}) \rightarrow \mathscr{P}(\mathbf{A}) = \mathbf{Q_k}\mathscr{P}(\hat{\mathbf{A}})\mathbf{Q_k^T} \tag{22}$$

$$\mathscr{P}(\mathbf{A^T})\mathbf{P_k} = \mathbf{P_k}\mathscr{P}(\hat{\mathbf{A}}^{\mathrm{T}}) \rightarrow \mathscr{P}(\mathbf{A}) = \mathbf{P_k}\mathscr{P}(\hat{\mathbf{A}})\mathbf{P_k^T} \tag{23}$$

when $\deg(\mathscr{P}) < k$. These properties follow from the Lanczos iteration (see Appendix A). To match the first $2k$ moments, the following condition between the reduced and unreduced model must be satisfied:

$$\hat{\mathbf{C}}\hat{\mathbf{A}}^{l+j}\hat{\mathbf{B}} = \mathbf{C}\mathbf{A}^{l+j}\mathbf{B} \tag{24}$$

for $0 \leqslant l \leqslant k-1$ and $0 \leqslant j \leqslant k$. By using the properties shown in Equations (22) and (23) it can be shown that condition (24) is satisfied

$$\mathbf{C}\mathbf{A}^{l+j}\mathbf{B} = \mathbf{C}\mathbf{A}^{l}\mathbf{A}^{j}\mathbf{B} \tag{25}$$

$$= (\mathbf{C}\mathbf{Q_k}\hat{\mathbf{A}}^{l}\mathbf{Q_k^T})(\mathbf{P_k}\hat{\mathbf{A}}^{j}\mathbf{P_k^T}\mathbf{B}) \tag{26}$$

$$= \mathbf{C}\mathbf{Q_k}\hat{\mathbf{A}}^{l}\hat{\mathbf{A}}^{j}\mathbf{Q_k^{-1}}\mathbf{B} \tag{27}$$

$$= \hat{\mathbf{C}}\hat{\mathbf{A}}^{l+j}\hat{\mathbf{B}} \tag{28}$$

Thus the Lanczos method, by producing the biorthonormal matrices $\mathbf{P_k}$ and $\mathbf{Q_k}$, matches the first $2k$ moments of $H(s)$.

3.2. Implicitly restarted Lanczos

The Lanczos procedure requires starting vectors to start the iteration. The following starting vectors appear to give good results for model reduction problems [10]:

$$\mathbf{q_1} = \mathbf{B}/\sqrt{|\mathbf{CB}|} \tag{29}$$

$$\mathbf{p_1} = \mathrm{sign}(\mathbf{CB})\mathbf{C}^{\mathrm{T}}/\sqrt{|\mathbf{CB}|} \tag{30}$$

However, these start vectors in combination with the reduction procedure might transform a stable, full system (i.e. the real part of all eigenvalues smaller than zero) into an unstable reduced system. To overcome the consequences of a poor starting vector to construct the reduced model, one could explicitly remove the unstable eigenvalue λ_{u} from the reduced model by choosing new starting vectors, i.e. $\tilde{\mathbf{q_1}} = (\mathbf{A} - \lambda_{\mathrm{u}}\mathbf{I})\mathbf{q_1}$ and $\tilde{\mathbf{p_1}} = (\mathbf{A} - \lambda_{\mathrm{u}}\mathbf{I})\mathbf{p_1}$, and repeat the whole Lanczos process for k additional steps [10]. However, one could also implicitly modify the matrices $\mathbf{Q_k}$ and $\mathbf{P_k}$ and pass immediately to a stable version of the reduced model $\hat{\mathbf{A}} = \mathbf{P_k^T}\mathbf{A}\mathbf{Q_k}$. This implicit procedure is described in Grimme *et al.* [10] and is used here to speed up the reduction process.

3.3. Shifted Lanczos

A disadvantage of the Lanczos method is that breakdowns of the method (i.e. a division by zero) can occur under some circumstances. Looking at the Algorithm 1 in Appendix A we can see that

DOI: 10.1002/fld

this will occur when β_j or γ_j are zero. For the problem we are looking at here—obtaining a flame transfer function, in which a convective component is included between the location where the excitation occurs and the response location—β_1 and γ_1 are already zero, or at least very small, at the beginning of the algorithm. The value β_1 is defined as the product of the matrices **B** and **C**. The matrix **B** contains only values at the excitation location, while the matrix **C** contains only values at the response location. So when these matrices are multiplied, the result is zero and the Lanczos method breaks down.

Another disadvantage of the method is that there may be a large steady-state error, as the Lanczos method approximates the expansion of the transfer function around a frequency which is equal to infinity. With the shifted Lanczos method, this problem can be overcome. Moreover, it also solves the breakdown problem.

To obtain a good approximation around a certain frequency σ, the transfer function $H(s) = \mathbf{C}(s\mathbf{I} - \mathbf{A})^{-1}\mathbf{B}$ ($D = 0$) is expanded in a Taylor series around $s = \sigma = 2\pi f$

$$H(s) = \sum_{j=0}^{\infty} \eta_j(\sigma)(s - \sigma)^j \tag{31}$$

where $\eta_j(s = \sigma)$ are the moments of the power series

$$\eta_j(s = \sigma) \equiv \mathbf{C}(\mathbf{A} - \sigma\mathbf{I})^{-j}(\sigma\mathbf{I} - \mathbf{A})^{-1}\mathbf{B} \tag{32}$$

When comparing the moments $\eta_j(s = \sigma)$ (Equation (32)) with the moments that are matched with the standard Lanczos method (Equation (21)) it can be seen that a realization around any frequency σ can be obtained by replacing the matrix **A** in the standard Lanczos method with the shifted matrix $(\mathbf{A} - \sigma\mathbf{I})^{-1}$ and the vector **B** with $(\sigma\mathbf{I} - \mathbf{A})^{-1}\mathbf{B}$. This is the basis of the shifted Lanczos method [12].

Because the inverse of the square matrix $(\sigma\mathbf{I} - \mathbf{A})$ is a full matrix, the multiplication $(\sigma\mathbf{I} - \mathbf{A})^{-1}\mathbf{B}$ results in a full vector, and therefore the product **CB** cannot be zero anymore. This prevents breakdown of the method.

Real and imaginary shift frequencies can be used. Even multiple shift frequencies are possible [12], but require a large amount of extra CPU time and memory. This extra CPU time comes from the fact that in the shifted Lanczos method, the **A** matrix is now replaced by $(\mathbf{A} - \sigma\mathbf{I})^{-1}$, which now requires solving systems of linear equations instead of simple matrix–vector multiplications. Obviously, due to memory limitations this inverse matrix cannot be calculated explicitly when the dimension of **A** is large. The inverse operation is therefore applied by solving triangular systems obtained from an initial lower-upper (LU) decomposition (the linear system can also be solved iteratively). The number of triangular systems that need to be solved is equal to two times the order of the reduced model (see Algorithm 1 in Appendix A). The number of required LU factorizations is equal to the number of shift points used. Since the LU factorization is the most expensive operation in terms of CPU time and memory, using multiple shift points is less attractive when working with large-scale systems. Therefore, a single shift point will be used here. Because the approximated transfer functions are in fact low-pass filters (i.e. a lot of information in the low-frequency region), a shift frequency of 1 Hz is used in this paper.

DOI: 10.1002/fld

4. VALIDATION LINEAR COEFFICIENT METHOD

The performance of the linear coefficient method is demonstrated by calculating the flame transfer function of a simple combustion system (for more examples of the application of the state-space system to discretized systems, see [5]). To do so, a linear representation of the CFD equations at all mesh nodes has to be extracted. Use is made of a commercial CFD code, that renders the steady-state solution of the RaNS equations and the combustion scalar equations. Unfortunately for our method, for reason of computational stability the CFD equations are not solved as a whole in the CFD code. The transport equations are distributed over multiple groups and group-wise solved in several iteratively coupled loops. Due to this it is not possible to directly output the coefficients. Therefore, the discretization and the equations which are used in the CFD code were implemented in MATLAB. To calculate the coefficients it is not necessary to use multiple loops over the equations for computational stability. By importing the mesh and the variable values from a steady-state converged solution, the coefficients of the state-space matrices can be calculated by monitoring how the time derivatives change when the steady-state values of the independent variables are slightly changed. For example, the coefficient a_{ij} of the **A** matrix can be obtained by changing variable j with a value $\Delta\psi_j$ and calculating the response of the time derivative of variable i, according to

$$a_{ij} = \frac{\mathrm{d}\psi_i'}{\mathrm{d}t} \Big/ \Delta\psi_j \tag{33}$$

To test the method, a circular combustion chamber is considered (Figure 4). The geometry is based on a test rig that was built in the framework of the EU project DESIRE at the University of Twente. A radial swirl burner provides a swirling flow, which stabilizes the flame.

In the example problem, only the grey part of Figure 4 is modelled. The boundary conditions at the inlet of this reduced model come from a simulation with the full geometry. The model is further reduced by only considering a 10° cut of the circular geometry and imposing periodic boundary conditions at both radial planes to account for the remainder of the circular combustor.

The model is meshed with an unstructured mesh of 70 907 elements (21 289 nodes). Most of these elements are concentrated in the flame zone. The mesh is dense enough to finally yield a flame transfer function that is mesh independent. In this simulation 11 transport equations are solved: 3 momentum equations, 1 mass balance equation, 2 turbulence equations for k and ε, 1 energy

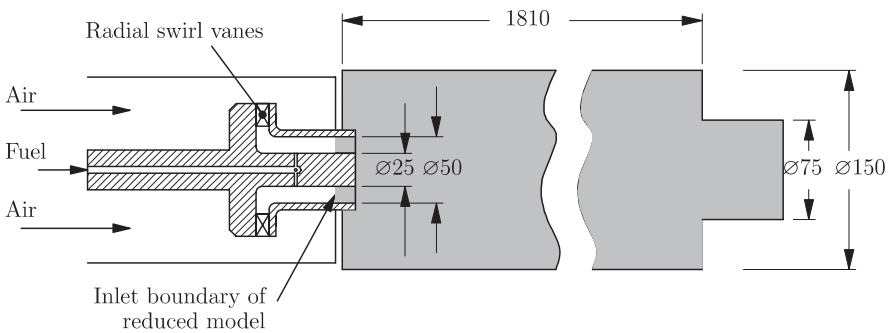

Figure 4. Reduced model for example calculation (dimensions in mm).

DOI: 10.1002/fld

Table I. Operating point for the test-case.

Thermal power (kW)	Equivalence ratio (dimensionless)	Preheating temperature (K)	Adiabatic flame temperature (K)	Absolute pressure (bar)
150	0.56	373	1661	1.5

equation and 4 convection–diffusion equations for the transport of the species mass fractions (CH_4, O_2, CO_2 and H_2O).

The CFD problem described above was solved using the coupled, unstructured solver of CFX 5.6. The inlet conditions used in this test case are listed in Table I.

It is assumed that the fuel is perfectly mixed with air at the inlet of the model. This allows to solely fluctuate the equivalence ratio, which is for most combustion systems the principal cause for inducing heat release rate perturbations [13, 14]. The flame transfer function between the change of the volume-integrated heat release rate with a change in the equivalence ratio ϕ is determined in several transient simulations, using impulse excitation in the equivalence ratio. White noise excitation would give more accurate results than impulse excitation, but requires (far) more computational effort [5]. The transient CFD simulations serve as a validation for the results obtained with the linear coefficient method. The simulations are done with two different time steps: 0.5 and 0.25 ms. These time step sizes are both small enough to result in fully converged solutions at each new time level.

To include the excitation in the state-space matrices of the linear coefficient method, it should first be expressed in terms of the independent variables. For this purpose, the equivalence ratio perturbation can be expressed as a linear combination of the mass fractions y_{CH_4} and y_{O_2} at the inlet. Since the coefficients of these two independent variables are already calculated in the **A** matrix, the coefficients of the **B** matrix can be constructed from it.

The response of the dynamic model, i.e. the volume-integrated heat release rate, is represented in the state-space model by the **C** and D matrices (see Equation (7)). The coefficients of the **C** matrix give the relationship between a fluctuation in the volume-integrated heat release rate and the independent variables, i.e.

$$c_j = \frac{Q^{\text{new}} - Q^{\text{s}}}{\Delta\psi_j} \tag{34}$$

The integrated heat release rate Q is a global variable, so the **C** matrix is one dimensional. The superscripts s and new indicate the steady, unperturbed situation, and the perturbed situation, respectively. In practice, the matrix is calculated by looping over all independent variables, perturbing the variable, and monitoring the change in the volume-integrated heat release rate as a result of the perturbation. After calculating the **C** matrix, the D matrix can be calculated from it in the same way as the **B** matrix can be calculated from the **A** matrix.

For the flow field, it is required to put the outlet at a location where the gradients in the flow are small. However, in the linear coefficient method one is only interested in the heat release rate response. Since acoustic pressure and velocity fluctuations have very little influence on the heat release rate [15], only convective effects in the flow field can influence the heat release rate. Therefore, it makes sense to omit all coefficients corresponding to axial locations beyond the closing position of the inner recirculation zone. This way, the number of nodes in the linear

DOI: 10.1002/fld

coefficient method could be reduced from 21 289 to 3923. With 11 independent variables per node, the order of the linear coefficient model becomes 43 153. Using the Lanczos method, the state-space model was further reduced to order 25, prior to calculating the transfer function, i.e. a reduction of over 99.9%.

First, only fluctuations in the 4 convection–diffusion equations for the mass fractions are considered. The influence of the other equations and independent variables is removed by keeping them at a constant value in the transient simulation. The transfer functions determined with impulse excitation in a transient simulation and with the linear coefficient method are compared in Figure 5 (for an explanation of the shape of this transfer function in relation to flame and flow properties, see [5]). All transfer functions presented in this paper are made dimensionless by scaling them with their mean counterparts.

Figure 5 shows that when the time step is decreased, the results obtained from impulse excitation in CFX are increasingly approximating the linear coefficient result. This confirms the statement that transfer functions obtained with the linear coefficient method do not suffer from time truncation errors. The transfer functions still look very simple, which is due to the fact that only the convection and diffusion of the species are considered here. Adding more equations will influence the flame transfer functions.

When the enthalpy equation is added to the considered set of equations, the transfer functions shown in Figure 6 are obtained.

The enthalpy equation largely influences the results. This is because it directly influences the temperature, which in turn has a large influence on the reaction rate. While the cut-off frequency remains more of less the same as with the 4 convection–diffusion equations, additional bumps appear on the spectrum. It is also seen that at some frequencies, the error made with the transient CFD method is large, even with the smallest considered time step.

Finally, the transfer function of the entire model is compared with the transient results in Figure 7.

Some influence of the hydrodynamical equations can be noted when comparing Figure 7 with the previously obtained transfer functions. However, the influence is not large. By considering only

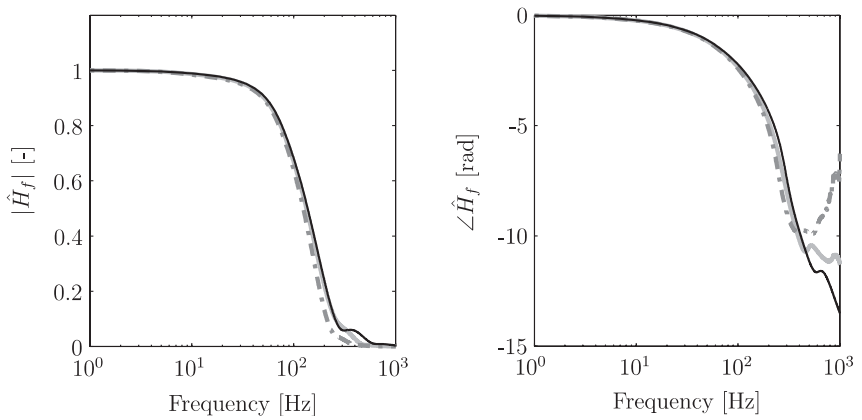

Figure 5. Comparison between transfer functions obtained from impulse excitation in CFX and from the linear coefficient method. Only the 4 convection–diffusion equations for the mass fractions are included. —, linear coefficient method; _ _, transient CFD $\Delta t = 5e-4$ s; ——, transient CFD $\Delta t = 2.5e-4$ s.

DOI: 10.1002/fld

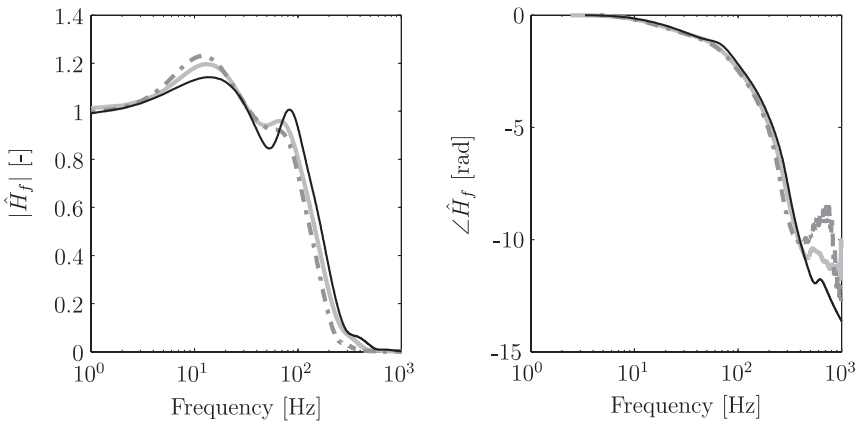

Figure 6. Comparison between transfer functions obtained from impulse excitation in CFX and from the linear coefficient method. The 4 convection–diffusion equations for the mass fractions and the enthalpy equation are included. —, linear coefficient method; _ _, transient CFD $\Delta t = 5e-4$ s; ——, transient CFD $\Delta t = 2.5e-4$ s.

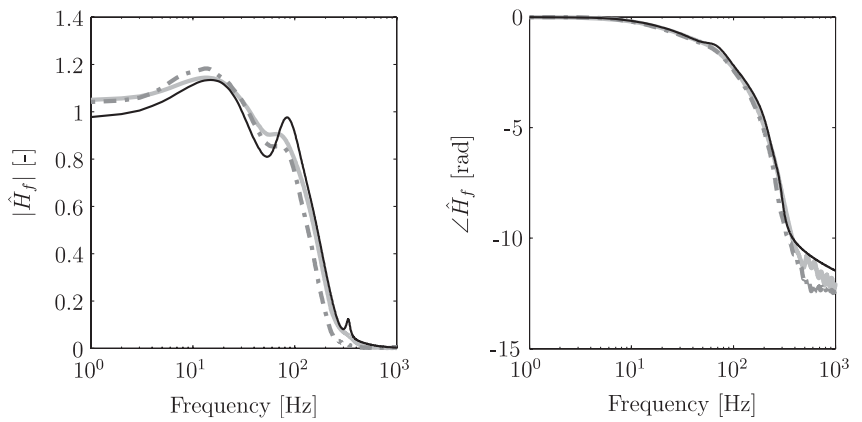

Figure 7. Comparison between transfer functions obtained from impulse excitation in CFX and from the linear coefficient method. All equations are included. —, linear coefficient method; _ _, transient CFD $\Delta t = 5e-4$ s; ——, transient CFD $\Delta T = 2.5e-4$ s.

the enthalpy and the 4 convection–diffusion equations, already a very good description of the flame transfer function for this case is obtained.

Additionally, an axi-symmetric formulation of the linear coefficient method was compared here with the three-dimensional formulation on basis of the geometry with the 10° cut. The axi-symmetric formulation only requires the inclusion of the nodes at one periodic boundary. The total order of the state-space model for the 11 equations is now further reduced to 15 257 (1387 nodes considered). Figure 8 shows a comparison between the results obtained with a two-dimensional implementation and the transient CFD results.

DOI: 10.1002/fld

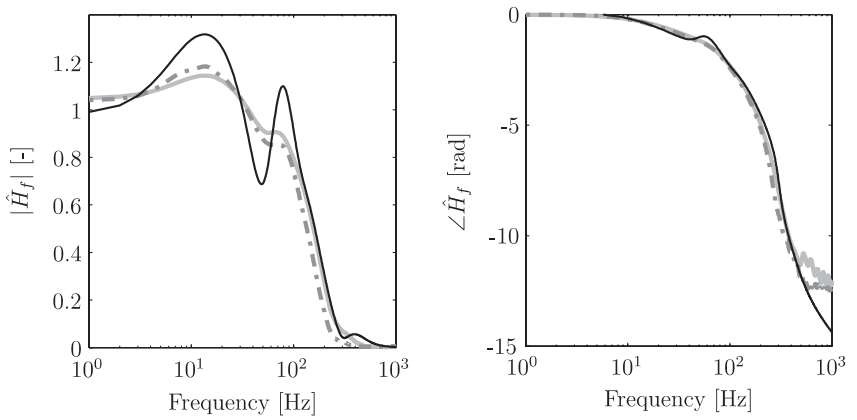

Figure 8. Comparison between transfer functions obtained from impulse excitation in CFX and from the two-dimensional version of the linear coefficient method. All equations are included. —, linear coefficient method; _ _, transient CFD $\Delta t = 5e{-}4$ s; ——, transient CFD $\Delta t = 2.5e{-}4$ s.

Table II. CPU times of state space and transient calculations (all preceded by retrieving a steady-state solution).

	CPU time (s)		
Element	4 equations	5 equations	11 equations
Impulse excitation CFX $\Delta t = 0.25$ ms	9.5×10^3	1.5×10^4	3.0×10^4
Reducing to order 25 with restarted and shifted Lanczos method	4.4×10^1	9.5×10^1	3.9×10^3
Calculated transfer function from reduced model	6	6	6

While the peaks occur at the same locations as the CFD results, the level is off. It appears to be very important that the steady-state solution obtained with CFX is mapped onto the same mesh in the linear coefficient method. Mapping the solution on a two-dimensional mesh results in slightly different residuals that cause the solution not to satisfy the steady-state condition anymore. Applying the linear coefficient method might then give a wrong solution.

In Table II, the CPU times are listed for each method. For relatively small size problems, the computational effort of the linear coefficient method is shown to be about a factor 10^2 less compared to impulse excitation (for this specific case). When the problems become larger, i.e. adding more equations or more nodes, this reduction in computational effort decreases slowly. The reason for this is that solving the large linear systems that occur in the shifted version of the Lanczos method, requires increasingly more calculation time.

When performing a transient simulation in CFX, each time step a similar sized linear problem is solved. The performance of the solver is greatly improved by employing multigrid techniques, i.e. incorporating information about the location of the nodes in the solving procedure. When employing similar solution techniques in the linear coefficient method, it should be possible to equal the time needed to reduce the system in size to $2k$ time steps ($2k$ linear systems are solved,

DOI: 10.1002/fld

see Section 3.3) in CFX, where k is the size of the reduced system. So when the problem is reduced to order 50, 100 linear systems are solved. When the iterative multigrid solver of CFX is used, this can in principle be done in the same amount of CPU time in which 100 time steps are done.

5. CONCLUSIONS

With the linear coefficient method, flame transfer functions are calculated using a linearization of the unsteady CFD equations around a steady-state solution. This is shown to be faster and more accurate than when using conventional transient methods and spectral analysis. Therefore, the method can be used as a design tool in determining the thermo-acoustic behaviour of combustion systems. Note that the applications of the method are not restricted to flame transfer function calculations. Any harmonic numerical experiment can be replaced by the linear coefficient method.

The test problems that have been studied with the linear coefficient method range up as high as order 45 000. For higher-order models, the currently used solution process necessary for solving the linear systems in the shifted Lanczos method becomes less efficient. To remove the limit in size, a multigrid solver should be used to solve the linear systems in the shifted Lanczos method. When the iterative multigrid solver of CFX would be used, the reduction of the linear description to order k can in principle be done in the same amount of CPU time in which $2k$ time steps are done.

APPENDIX A: THE GENERAL UNSYMMETRICAL LANCZOS METHOD

The explanation of the general unsymmetrical Lanczos method starts with the concept of Krylov spaces [11]. A Krylov matrix $\mathscr{K}$ is a matrix of the form

$$\mathscr{K}(\mathbf{A}, \mathbf{x}, n) = [\mathbf{x}, \mathbf{A}\mathbf{x}, \mathbf{A}^2\mathbf{x}, \ldots, \mathbf{A}^{n-1}\mathbf{x}] \tag{A1}$$

while the Krylov *space* is the space spanned by the columns of the Krylov matrix. Moreover, the Rayleigh quotient $r(\mathbf{x})$ is defined as

$$r(\mathbf{x}) = \frac{\mathbf{x}^{\mathrm{T}}\mathbf{A}\mathbf{x}}{\mathbf{x}^{\mathrm{T}}\mathbf{x}}, \quad \mathbf{x} \neq \mathbf{0} \tag{A2}$$

A property of the Rayleigh quotient is that its maximum and minimum values represent the maximum and minimum eigenvalue of $\mathbf{A}$, respectively [11]. These eigenvalues will be indicated as $\lambda_1(\mathbf{A})$ and $\lambda_n(\mathbf{A})$, respectively, in which n is the dimension of the square matrix $\mathbf{A}$.

Now assume that $\mathbf{q_i} \subseteq \Re^n$ is a sequence of orthonormal column vectors, and let $\mathbf{Q_k} = [\mathbf{q_1}, \ldots, \mathbf{q_k}]$. Using expression (A2) the largest eigenvalue M_k of the matrix $\mathbf{Q_k^{\mathrm{T}}AQ_k}$ can be written as

$$M_k = \lambda_1(\mathbf{Q_k^{\mathrm{T}}AQ_k}) = \max_{\mathbf{y}\neq 0} \frac{\mathbf{y}^{\mathrm{T}}(\mathbf{Q_k^{\mathrm{T}}AQ_k})\mathbf{y}}{\mathbf{y}^{\mathrm{T}}\mathbf{y}} = \max_{\|\mathbf{y}\|_2=1} r(\mathbf{Q_k}y) \leqslant \lambda_1(\mathbf{A}) \tag{A3}$$

In the Lanczos algorithm the key issue is to choose $\mathbf{Q_k}$ such that M_k is an increasingly better estimate of $\lambda_1(\mathbf{A})$. When $k<n$, this will result in a $k \times k$ matrix $\hat{\mathbf{A}} = \mathbf{Q_k^{\mathrm{T}}AQ_k}$, approximating the largest eigenvalues of the $n \times n$ matrix $\mathbf{A}$.

DOI: 10.1002/fld

When $\mathbf{q_{k+1}}$ is chosen such that

$$\text{span}\{\mathbf{q_1}, \ldots, \mathbf{q_{k+1}}\} = \text{span}\{\mathbf{q_1}, \mathbf{Aq_1}, \ldots, \mathbf{A}^{k-1}\mathbf{q_1}, \mathbf{A}^k\mathbf{q_1}\} \tag{A4}$$

it is ensured that the new approximation of the largest eigenvalue is better than the previous one [11]. This is because the added vector $\mathbf{q_{k+1}}$ is then chosen such that the vector space span of $\mathbf{Q_{k+1}}$ contains the direction in which the gradient of the Rayleigh quotient increases most rapidly, since

$$\nabla r(\mathbf{x}) = \frac{2}{\mathbf{x}^T\mathbf{x}}(\mathbf{Ax} - r(\mathbf{x})\mathbf{x}) \in \text{span}\{\mathbf{x}, \mathbf{Ax}\} \tag{A5}$$

This means that when the space spanned by projector matrix $\mathbf{Q_k}$ is taken equal to the Krylov space of $\mathscr{K}(\mathbf{A}, \mathbf{q_1}, k)$, the eigenvalues of the reduced $k \times k$ matrix $\mathbf{Q_k^T A Q_k}$ will be progressively better approximation of the original matrix' eigenvalues. The Lanczos method is used to efficiently compute the orthonormal basis for this Krylov subspace.

The projected matrix $\hat{\mathbf{A}} = \mathbf{Q_k^T A Q_k}$ is assumed to be tridiagonal, i.e. a square matrix with non-zero coefficients only on the diagonal and horizontally or vertically adjacent the diagonal. This allows an inexpensive calculation of the eigenvalues of $\hat{\mathbf{A}}$ once the orthonormal matrix $\mathbf{Q_k}$ is found. The elements of the tridiagonal matrix $\hat{\mathbf{A}}$ can be computed in a direct way by setting $\mathbf{Q_k} = [\mathbf{q_1}, \ldots, \mathbf{q_k}] = [\mathbf{q_1}, \mathbf{Aq_1}, \ldots, \mathbf{A}^k\mathbf{q_1}]$ and:

$$\hat{\mathbf{A}} = \mathbf{Q_k^T A Q_k} = \mathbf{Q_k^{-1} A Q_k} = \begin{bmatrix} \alpha_1 & \gamma_1 & 0 & 0 & 0 \\ \beta_1 & \alpha_2 & . & 0 & 0 \\ 0 & . & . & . & 0 \\ 0 & 0 & . & . & \gamma_{k-1} \\ 0 & 0 & 0 & \beta_{k-1} & \alpha_k \end{bmatrix} \tag{A6}$$

For clarity, the inverse transpose of the $\mathbf{Q_k}$ matrix is denoted as $\mathbf{P_k}$, i.e. $\mathbf{Q_k^{-T}} \equiv \mathbf{P_k}$. The $\mathbf{Q_k}$ and $\mathbf{P_k}$ matrices consist of k vectors:

$$\mathbf{Q_k} = [\mathbf{q_1}, \ldots, \mathbf{q_k}] \tag{A7}$$

$$\mathbf{P_k} = [\mathbf{p_1}, \ldots, \mathbf{p_k}] \tag{A8}$$

When comparing columns in $\mathbf{AQ_k} = \mathbf{Q_k}\hat{\mathbf{A}}$ and $\mathbf{A^T P_k} = \mathbf{P_k}\hat{\mathbf{A}}^T$ it is found that

$$\mathbf{Aq_i} = \gamma_{i-1}\mathbf{q_{i-1}} + \alpha_i\mathbf{q_i} + \beta_i\mathbf{q_{i+1}}, \quad \gamma_0\mathbf{q_0} \equiv 0 \tag{A9}$$

$$\mathbf{A^T p_i} = \beta_{i-1}\mathbf{p_{i-1}} + \alpha_i\mathbf{p_i} + \gamma_i\mathbf{p_{i+1}}, \quad \beta_0\mathbf{p_0} \equiv 0 \tag{A10}$$

for $i = 1, \ldots, k-1$. The biorthonormality condition $\mathbf{P_k^T Q_k} = \mathbf{Q_k^{-1} Q_k} = \mathbf{I_k}$ implies $\alpha_i = \mathbf{p_i^T A q_i}$ and

$$\beta_i\mathbf{q_{i+1}} \equiv \mathbf{r_i} = (\mathbf{A} - \alpha_i\mathbf{I})\mathbf{q_i} - \gamma_{i-1}\mathbf{q_{i-1}} \tag{A11}$$

$$\gamma_i\mathbf{p_{i+1}} \equiv \mathbf{s_i} = (\mathbf{A} - \alpha_i\mathbf{I})^T\mathbf{p_i} - \beta_{i-1}\mathbf{p_{i-1}} \tag{A12}$$

Note that $1 = \mathbf{p_{i+1}^T q_{i+1}} = (\mathbf{s_i}/\gamma_i)^T(\mathbf{r_i}/\beta_i)$ so that $\gamma_i = \mathbf{s_i^T r_i}/\beta_i$. In the variant of the Lanczos method that is used here, β_i is set to $\sqrt{|\mathbf{s_i^T r_i}|}$, so that $\gamma_i = \text{sign}(\mathbf{s_i^T r_i})\beta_i$.

DOI: 10.1002/fld

The algorithm for obtaining the biorthogonormal matrices $\mathbf{Q_k}$ and $\mathbf{P_k}$ is given.

Algorithm 1 General unsymmetrical Lanczos method.

$\beta_1 = \sqrt{|\mathbf{CB}|}$
$\gamma_1 = \text{sign}(\mathbf{CB})\beta_1$
$\mathbf{q_1} = \mathbf{B}/\beta_1$
$\mathbf{p_1} = \mathbf{C}^T/\gamma_1$
$\mathbf{q_0} = \mathbf{0}$
$\mathbf{p_0} = \mathbf{0}$
for $i = 1$ to k **do**
  $\alpha_i = \mathbf{p_i}^T \mathbf{A} \mathbf{q_i}$
  $\mathbf{r_i} = (\mathbf{A} - \alpha_i \mathbf{I})\mathbf{q_i} - \gamma_i \mathbf{q_{i-1}}$
  $\mathbf{s_i} = (\mathbf{A} - \alpha_i \mathbf{I})^T \mathbf{p_i} - \beta_i \mathbf{p_{i-1}}$
  $\beta_{i+1} = \sqrt{|\mathbf{s_i}^T \mathbf{r_i}|}$
  $\gamma_{i+1} = \text{sign}(\mathbf{s_i}^T \mathbf{r_i})\beta_{i+1}$
  $\mathbf{q_{i+1}} = \mathbf{r_i}/\beta_{i+1}$
  $\mathbf{p_{i+1}} = \mathbf{s_i}/\gamma_{i+1}$
end for

Using this algorithm, the matrices $\mathbf{Q_k}$, $\mathbf{P_k}$ $(= \mathbf{Q_k^{-T}})$ and $\hat{\mathbf{A}}$ can be calculated iteratively. The extremal eigenvalues of $\hat{\mathbf{A}}$ turn out to be very good approximations of the extremal eigenvalues of $\mathbf{A}$. It can be seen that the start the starting vectors $\mathbf{q_1}$ and $\mathbf{p_1}$ of the Lanczos procedure are given by

$$\mathbf{q_1} = \mathbf{B}/\sqrt{|\mathbf{CB}|} \tag{A13}$$

$$\mathbf{p_1} = \text{sign}(\mathbf{CB})\mathbf{C}^{\mathrm{T}}/\sqrt{|\mathbf{CB}|} \tag{A14}$$

This appears to give good results for model reduction problems [10].

ACKNOWLEDGEMENTS

This work is performed in the framework of the EU supported project DESIRE, which includes the following partners: Siemens, DLR, CERFACS, KEMA, CIMNE, E.ON and the University of Twente. Moreover, the authors want to thank Dr Ian P. Jones of CFX Ansys for his support and CFX Ansys for the use of the software.

REFERENCES

1. Külsheimer C, Büchner H. Combustion dynamics of turbulent swirling flames. *Combustion and Flame* 2002; **131**:70–84.
2. Bernier D, Ducruix S, Lacas F, Candel S, Robart N, Poinsot T. Transfer function measurements in a model combustor: application to adaptive instability control. *Combustion Science and Technology* 2003; **175**:993–1013.
3. Paschereit CO, Schuermans B, Polifke W, Mattson O. Measurement of transfer matrices and source terms of premixed flames. *Journal of Engineering for Gas Turbines and Power* 2002; **124**:239–247.
4. Lieuwen TC. Investigation of combustion instability mechanisms in premixed gas turbines. *Ph.D. Thesis*, Georgia Institute of Technology, 1999.
5. van Kampen JF. Acoustic pressure oscillations induced by confined turbulent premixed natural gas flames. *Ph.D. Thesis*, University of Twente, 2006. Available at http://purl.org/utwente/55987

DOI: 10.1002/fld

6. Lieuwen T. *Physics of Premixed Combustion-Acoustic Wave Interactions* (Chapter 12: Operational Experience, Fundamental Mechanisms, and Modeling), Lieuwen T, Yang V (eds), vol. 210. Combustion Instabilities in Gas Turbine Engines. American Institute of Aeronautics and Astronautics: U.S.A., 2005.
7. Gentemann A, Hirsch C, Kunze K, Sattelmayer T, Polifke W. Validation of flame transfer function reconstruction for perfectly premixed swirl flames. *Proceedings of ASME Turbo Expo 2004. 2004 Power for Land, Sea, and Air*, Vienna, Austria, vol. GT2004-53776, 14–17 June 2004.
8. Antoulas AC, Sorensen DC. Approximation of large-scale dynamical systems: an overview. *International Journal of Applied Mathematics Computer Science* 2001; **11**(5):1093–1121.
9. Baj Z. Krylov subspace techniques for reduced-order modeling of large-scale dynamical systems. *Applied Numerical Mathematics* 2002; **43**:9–44.
10. Grimme EJ, Sorensen DC, van Dooren P. Model reduction of state space systems via an implicitly restarted Lanczos method. *Numerical Algorithms* 1995; **12**:1–31.
11. Golub GH, van Loan CF. *Matrix Computations* (3rd edn). The Johns Hopkins University Press: Baltimore, MD, 1996.
12. Gallivan K, Grimme E, van Dooren P. A rational Lanczos algorithm for model reduction. *Numerical Algorithms* 1996; **12**(1–2):33–63.
13. Hubbard S, Dowling AP. Acoustic resonances of an industrial gas turbine combustion system. *Journal of Engineering for Gas Turbines and Power* 2001; **123**(4):766–773.
14. Cheung WS, Sims GJM, Copplestone RW, Tilston JR, Wilson CW, Stow SR, Dowling AP. Measurement and analysis of flame transfer function in a sector combustor under high pressure conditions. *Proceedings of ASME Turbo Expo 2003*, *2003-GT-38219*, 2003; 1–8.
15. Lieuwen TC, Neumeier Y, Zinn BT. The role of unmixedness and chemical kinetics in driving combustion instabilities in lean premixed combustors. *Combustion Science and Technology* 1998; **135**:193–211.

DOI: 10.1002/fld